

RSC Advances



This is an *Accepted Manuscript*, which has been through the Royal Society of Chemistry peer review process and has been accepted for publication.

Accepted Manuscripts are published online shortly after acceptance, before technical editing, formatting and proof reading. Using this free service, authors can make their results available to the community, in citable form, before we publish the edited article. This *Accepted Manuscript* will be replaced by the edited, formatted and paginated article as soon as this is available.

You can find more information about *Accepted Manuscripts* in the [Information for Authors](#).

Please note that technical editing may introduce minor changes to the text and/or graphics, which may alter content. The journal's standard [Terms & Conditions](#) and the [Ethical guidelines](#) still apply. In no event shall the Royal Society of Chemistry be held responsible for any errors or omissions in this *Accepted Manuscript* or any consequences arising from the use of any information it contains.

Cite this: DOI: 10.1039/c0xx00000x

www.rsc.org/xxxxxx

PAPER

A smart artificial glutathione peroxidase with temperature responsive activity constructed by host-guest interaction and self-assembly

Yanzhen Yin,^{a*} Shufei Jiao^a, Chao Lang,^b Junqiu Liu^{b*}

Received (in XXX, XXX) Xth XXXXXXXXX 20XX, Accepted Xth XXXXXXXXX 20XX

DOI: 10.1039/b000000x

A smart supramolecular artificial glutathione peroxidase (GPx) with tunable catalytic activity was prepared based on host-guest interaction and a blending process. The functional guest molecules ADA-Te with catalytic center, ADA-Arg with binding site and the cyclodextrin-containing host polymers (CD-PNIPAMs) were first synthesized. The artificial glutathione peroxidase was constructed by host-guest interaction of ADA-Te and series of CD-PNIPAMs with different molecular weights. Through altering the molar ratio of building blocks (CD-PNIPAM₇₃, ADA-Te, ADA-Arg), the optimum artificial GPx (SGPx_{max}) with vesicles structure was prepared via a blending process. Significantly, SGPx_{max} displayed a noticeable temperature responsive catalytic activity and exhibited the typical saturation kinetics behavior as a real enzyme catalyst. It was proved that the change of the self-assembled structure of SGPx_{max} during the temperature responsive process played a significant role in altering the temperature responsive catalytic behavior. The construction of SGPx_{max} not only overcomes the insurmountable disadvantages existed in traditional supramolecular artificial GPxs but also bodes well for development of other biologically related functional supromolecular biomaterials.

Introduction

Reactive oxygen species (ROS) are the byproducts of cellular metabolism. The surplus ROS can lead to many human oxidative stress-related diseases¹⁻³. Generally, such oxidative stress-related diseases are controlled by the antioxidative defense system, especially by the antioxidative enzyme system. As a member of the family of antioxidative enzymes, glutathione peroxidase (GPx, Ec.1.11.1.9) is an important selenium-containing enzyme, which catalyzes the reduction of hydroperoxides (ROOHs) using glutathione (GSH) as substrate^{4,5}. Owing to its biologically crucial role, considerable efforts have been devoted to produce organoselenium/tellurium compounds that mimic the property of GPx in recent years⁶⁻¹². In our group, based on the understanding of the structure of native GPx, some artificial GPxs have been designed based on macromolecular scaffolds^{13-20,45}. Especially, considerable attentions have been drawn to artificial GPxs based on supramolecular scaffolds^{9,10,17,18,21,22}.

Generally, molecular self-assembly behavior is a general phenomenon in nature, which plays a pivotal role in biological functions^{23,24}. Being the alternative to the self-assembly structure in nature, versatile materials based on supramolecular chemistry have emerged as fascinating scaffolds for many interdisciplinary materials²⁵⁻³². Typically, supramolecular materials are extensively applied in the fields of protein supramolecular complexes^{33,34}, sensors³⁵⁻³⁷, controlled release systems³⁸⁻⁴¹, artificial enzymes^{18,21} as well as self-healing materials^{42,43}. The unique properties of reversible dynamic assembly behavior and simplified

construction process are all exhibited in these versatile materials. Specially, these unique properties are benefited to the construction of highly efficient supramolecular artificial GPxs (SGPxs). Liu and coworkers pioneered in the construction of the host SGPx with highly catalytic ability and strong substrate binding ability, which opened a new window for the preparation of artificial GPx based on supramolecular chemistry^{7,44}. Subsequently, by marrying the successfully host cyclodextrin GPx with versatile supramolecular building blocks, SGPxs based on giant nanotube²¹, protein nanowire⁹, protein nanodisk¹⁰, supramolecular microgel⁴⁵, hyperbranched supramolecular polymer¹⁸ and star-shaped pseudo-block copolymer¹⁹ were constructed. Similar to the traditional polymer scaffold for artificial enzyme, SGPxs were also proved to be endowed with the advantages of the simplified construction process as well as the enriched catalytic center^{46,47}. Although supramolecular self-assembled materials were excellent scaffolds for artificial GPx, there were still two serious disadvantages in these SGPxs. On the one hand, most of them were just endowed with the catalytic center of GPx, which was only one of the three catalytic factors functioned to maintain the high catalytic activity^{9,10,19}. It was a pity that the binding sites were usually absence, which could not accurately mimic the catalysis and recognition of native GPx. On the other hand, even if the binding sites and catalytic center were both anchored into a few of SGPxs, the intelligent alteration of substrate binding ability and catalytic ability could not be achieved^{18,21}. It was known that only surplus ROS led to many human oxidative stress-related diseases and appropriate amount of ROS commonly acted as signal molecules in the metabolism^{1,3}.

The absence of adjustable and intelligent catalytic ability in **SGPx** has largely limited the further investigation and application of artificial GPx. Therefore, how to overcome these two disadvantages, design a novel **SGPx** with adjustable catalytic ability and bearing enriched catalytic factors (catalytic center and substrate binding sites) is still a great challenge.

Blending process is a versatile strategy exploited for the development of new polymeric materials with property profiles superior to those of the individual components^{20,48-50}. The unique property of blending process can be employed to overcome the disadvantage of the absence of enriched catalytic factors. Moreover, in our previous reports, we also proved that the construction of smart artificial GPx with intelligent catalytic ability was achievable using traditional single chain block copolymer and supramolecular microgel as scaffolds based on PNIPAM^{45,50}. Therefore, the application of the construction method from previous intelligent artificial GPx in the development of novel **SGPx** is desirable. It can overcome the disadvantage of absence of the intelligent catalytic ability in previous **SGPx**s. Additionally, the host-guest interaction between cyclodextrin and adamantane has been proved to be the efficient non-covalent interaction for the construction of supramolecular materials⁴²⁻⁵¹,

Herein, we designed a novel smart **SGPx** combining PNIPAM scaffold, host-guest interaction self-assembly and blending process. Typically, as a novel smart artificial GPx, **SGPx_{max}** displayed a noticeable temperature responsive catalytic activity and the typical saturation kinetics behavior as a real enzyme catalyst. To the best of our knowledge, this is the first example of the successful construction of smart artificial GPx based on host-guest interaction and a blending process. We anticipate that this artificial GPx not only bodes well for the exploration of intelligent antioxidant drugs but also highlights the development of host-guest self-assembled supramolecular materials.

Experimental Section

Materials

Tris(2-aminoethyl)amine (TREN, Acros) was used as received. Tris(2-dimethylaminoethyl)amine (Me₆TREN) was synthesized as described previously⁵². *N*-isopropylacrylamide (NIPAM) (Aldrich) was recrystallized from hexane and toluene, and dried under a vacuum prior to use. Sodium borohydride, 1-adamantanecarbonyl chloride, and 3-bromo-1-propanol were purchased from Fluka and were used without further purification. Cumene hydroperoxide (CUOOH), H₂O₂, and 4-nitrobenzenethiol (NBT) were purchased from J&K Scientific Ltd. 3-carboxyl-4-nitrobenzenethiol (TNB) was synthesized from 5,5'-dithiobis(2-nitrobenzoic acid) as described previously⁷. Acrylamide, L-Arginine, 1-adamantanecarbonyl chloride, tellurium powder, β -cyclodextrin, phenyl methanol and 4-toluene sulfonyl chloride were purchased from Shanghai Reagent Co. Acryloyl chloride and propargyl alcohol were purchased from Anhui Wotu Reagent Co. 2-bromopropanol bromide was purchased from Lancaster. Triethylamine and tetrahydrofuran were rigorously dried with sodium. 1-[p-(phenyl-azo)phenoxyethyl]pyridinium bromide (**AZO**) was endowed from

liu's group (**AZO**: ¹H NMR (300 MHz, (CD₃)₂SO) δ (ppm) 9.17 (d, 2H), 8.66 (t, 1H), 8.21 (t, 2H), 7.90–7.81 (m, 4H), 7.60–7.52 (m, 3H), 7.13 (d, 2H), 5.10 (t, 2H), 4.65 (t, 2H)).

Instrumentations

The characterization of the structures of the compounds was performed with Bruker 300MHz spectrometer using a TMS proton signal as the internal standard. UV-vis spectra were obtained using a Shimadzu 2450 UV-vis-NIR spectrophotometer. Scanning electron microscopy (SEM) observations were carried out on a JEOL JSM-6700F scanning electron microscope with primary electron energy of 3kV. Transmission electron microscopy (TEM) observations were carried out on a JEOL JEM 3010 scanning electron microscope. The buffer pH values were determined with a METTLER TOLEDO 320 pH meter. Dynamic light scattering experiments were performed at Malven ZETAS12-ERNANOSERIES instrument. Molecular weights and molecular weight distributions were determined by GPC using THF as eluent at a flow rate of 1.0mL/min. The synthesis of **ADA-Te**, **ADA-Arg**, **CD-Br** were given in ESI. **CD-PNIPAM**s were synthesized according to the polymerization procedure reported by Masci et al⁵³. The detailed synthesis process was available in ESI.

Determination of the LCST

The determination of LCST was carried out according to the previous reported method⁵⁴. Typically, the optical transmissions of **CD-PNIPAM** solution (1 mg·mL⁻¹) at different temperatures were measured at 600 nm using a Shimadzu 2450 UV-vis-NIR spectrophotometer. Sample cells were thermostated in a circulator bath at different temperatures from 25 to 45°C prior to the measurements. The LCST was defined as the temperature of the 50% transmittance point during the first heating ramp.

Preparation of Te-CD-PNIPAM₇₃

The supramolecular building block **Te-CD-PNIPAM₇₃** with catalytic center of GPx was prepared based on **ADA-Te** and **CD-PNIPAM₇₃**. Typically, the preparation process was like this: **ADA-Te** (8.16 mg, 0.02 mmol) was dissolved in 0.20 mL DMF. **CD-PNIPAM₇₃** (196.3 mg, 0.02 mmol) was dissolved in 3.80 mL deionized water. Then, DMF solution of **ADA-Te** was slowly added into the solution of **CD-PNIPAM₇₃** under sonication at 25°C. After the dropwise process was finished, the mixture solution was treated under continual sonication at 25°C for 20 min. Then, the solution was removed by a rotary evaporator and the product was dried under vacuum for 24 h at 45°C. Finally, the dried product was dissolved in 10 mL PBS. And **Te-CD-PNIPAM₇₃** with the concentration of 2 mM was obtained.

Preparation of Arg-CD-PNIPAM₇₃

The preparation process of **Arg-CD-PNIPAM₇₃** was similar to that of **Te-CD-PNIPAM₇₃** except that **ADA-Te** was replaced by **ADA-Arg**. And **Arg-CD-PNIPAM₇₃** with the concentration of 2 mM was obtained.

Determination of GPx activity

The catalytic activity was assayed according to a modified method reported by Hilvert et al¹². Typically, the reaction was carried out at 36°C in a 1 mL quartz cuvette, 700 μ L of phosphate

buffer (pH=7.0, 50 mM) and 100 μ L of **SGPx_{max}** (10 μ M) were added, and then 100 μ L of the TNB solution (1.5 mM) was added. The mixture in the quartz cuvette was pre-incubated at appropriate temperature for 3 min. Finally, the reaction was initiated by the addition of 100 μ L of cumene hydroperoxide (CUOOH) (2.5 mM), and the absorption decrease of TNB at 410 nm (ϵ_{410} =13600 M⁻¹·cm⁻¹, pH=7.0) was monitored using a Shimadzu 2450 UV-vis-NIR spectrophotometer. Appropriate control of the non-enzymatic reaction was performed and was subtracted from the catalyzed reaction.

Results and Discussion

Construction of supramolecular building blocks for artificial GPx

The crystal structure of bovine erythrocyte glutathione peroxidase was reported by Epp et al in 1983⁴. And the catalytic site of GPx has been well studied. It was suggested that three important catalytic factors contributed to maintaining the efficient GPx catalytic activity: catalytic center, binding site, and hydrophobic cavity. Based on our previous studies, tellurium, arginine derivative and cyclodextrin were selected as efficient alternative catalytic factors in artificial GPx¹⁴⁻²⁰. As shown in Table 1, the description of abbreviation in this work was illustrated. As displayed in Fig. 1, **ADA-Te** with a similar function of selenocysteine was prepared as a catalytic center. **ADA-Arg** was responsible for the complexation of carboxyl groups of substrates as the binding site. Considering that ATRP was the efficient controlled polymerization for the synthesis of functional polymers^{55,56}, various cyclodextrin-containing host polymers (**CD-PNIPAMs**) with different molecular weights were synthesized by ATRP (see Fig. 2). GPC measurement displayed that their degree of polymerization (DPs) were estimated to be 73, 130, 374, respectively (see ESI). And the corresponding **CD-PNIPAMs** were denoted as **CD-PNIPAM₇₃**, **CD-PNIPAM₁₃₀**, **CD-PNIPAM₃₇₄**, respectively. Herein, **CD-Br** was the macroinitiator and contributed to anchoring the cyclodextrin into **CD-PNIPAMs**. Typically, the cyclodextrin end group in **CD-PNIPAMs** served as two purposes: on the one hand, it acted as host molecule for including guest molecules (**ADA-Te** or **ADA-Arg**) in the host-guest complex; on the other hand, the hydrophobic cavity of cyclodextrin in **SGPx** provided the hydrophobic microenvironment for the binding of hydrophobic substrates.

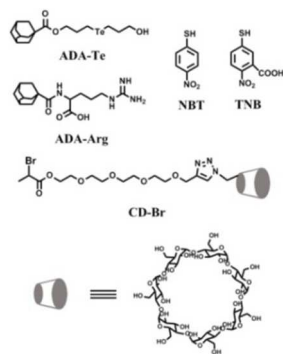


Fig. 1 The structures of the functional monomers **ADA-Te**, **ADA-Arg**, **CD-Br** and substrates (NBT, TNB)

Table 1 Description of abbreviation in this work

Abbreviation	description
GPx	glutathione peroxidase
ADA-Te	guest molecules with catalytic center (see Fig.1)
ADA-Arg	guest molecules with binding site (see Fig.1)
CD-PNIPAMs	cyclodextrin-containing host polymers(see Fig.2)
SGPxs	supramolecular artificial GPxs
AZO	1-[p-(phenyl-azo) phenoxyethyl]pyridinium bromide(see Scheme 2)
Te-CD-PNIPAM₇₃	complex of ADA-Te and CD-PNIPAM₇₃ .
Te-CD-PNIPAM₁₃₀	complex of ADA-Te and CD-PNIPAM₁₃₀
Te-CD-PNIPAM₃₇₄	complex of ADA-Te and CD-PNIPAM₃₇₄
Arg-CD-PNIPAM₇₃	complex of ADA-Arg and CD-PNIPAM₇₃ .
CD-Te-CD-PNIPAM₇₃	blend of CD-PNIPAM₇₃ and Te-CD-PNIPAM₇₃
Arg-Te-CD-PNIPAM₇₃	blend of Arg-PNIPAM₇₃ and Te-CD-PNIPAM₇₃
SGPx_{max}	optimum artificial GPx by blend of CD-PNIPAM₇₃ and Te-CD-PNIPAM₇₃

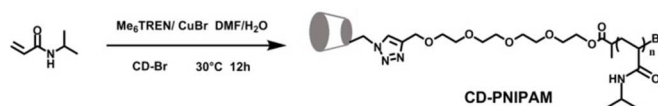
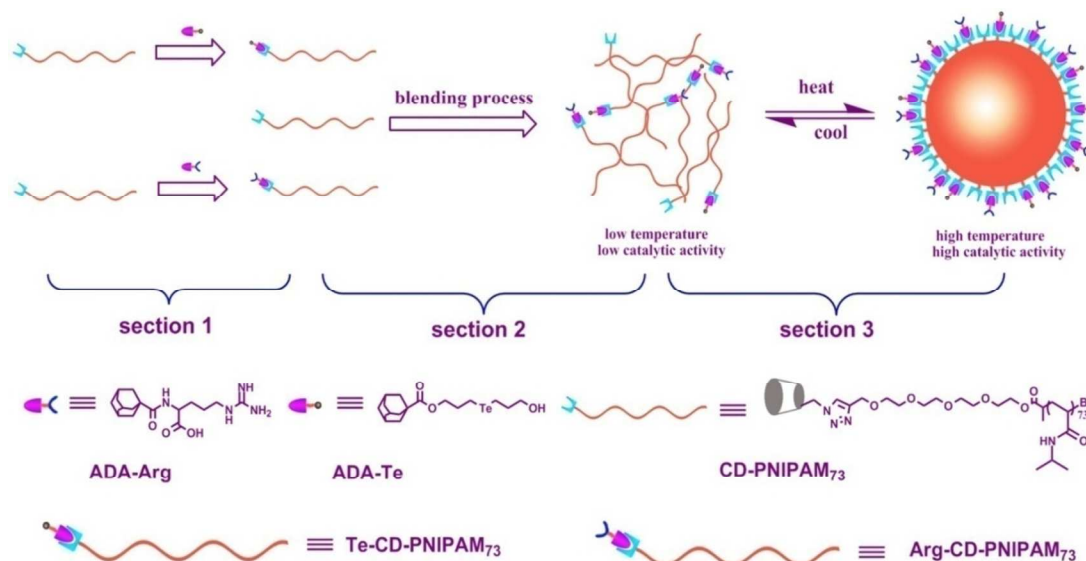


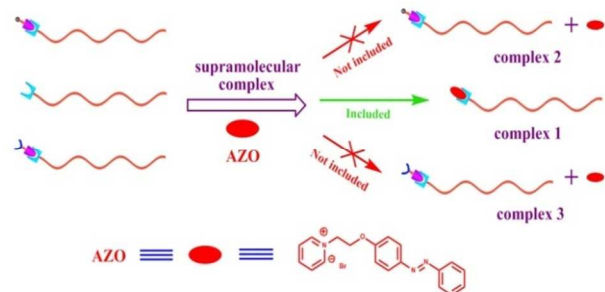
Fig. 2 Synthesis of **CD-PNIPAM**

PNIPAM undergoes a reversible volume phase transition at near-physiological temperature, which is a thermally sensitive polymer with a lower critical solution temperature (LCST) of 32°C⁵⁷⁻⁵⁸. Therefore, during the temperature responsive process, the soluble block copolymer bearing **PNIPAM** block can change to amphiphilic polymer when **PNIPAM** block shifts from being hydrophilic to hydrophobic. It provides the platform for the construction of versatile self-assembled materials^{16,59,60}. For **SGPx** in this work, the temperature responsive property of its **PNIPAM** scaffold plays an important role in the adjusting of catalytic activity. Based on the functional building blocks (**CD-PNIPAM₇₃**, **ADA-Te**, **ADA-Arg**), **SGPx** was constructed and illustrated in Scheme 1. Firstly, base on the host-guest interaction between adamantane (guest molecule in **ADA-Te** or **ADA-Arg**) and cyclodextrin (host molecule in **CD-PNIPAM**), the supramolecular building blocks (**Te-CD-PNIPAM₇₃**, **Arg-CD-PNIPAM₇₃**) with GPx catalytic factors were prepared and given in Scheme 1 section 1. Secondly, **SGPx_{max}** was constructed by a blending process (see Scheme 1 section 2). Finally, the reversible temperature responsive property of **SGPx_{max}** was illustrated in Scheme 1 section 3.



Scheme 1 A graphical representation of SGPx: **section 1**) the construction of supramolecular building blocks (**Te-CD-PNIPAM₇₃**, **Arg-CD-PNIPAM₇₃**); **section 2**) the construction of SGPx by a blending process; and **section 3**) the reversible temperature responsive behavior of SGPx

To prove the formation of host-guest complex in SGPx, NMR assay was carried out using **AZO** as an indicator. It is known that the host-guest complex between adamantane and cyclodextrin is remarkable stable. And the host-guest interaction between **AZO** and cyclodextrin is relative weak. Therefore, the graphical representation of the assumed competitive complex mechanism was given in Scheme 2.



Scheme 2 A graphical representation of the competitive complex mechanism using **AZO** as an indicator

To confirm this hypothesis, three groups of ¹H NMR spectra were characterized and illustrated in Fig. 3. Among three groups of ¹H NMR spectra, **complex 1** was the proton signals of aromatic rings in the binary system of **AZO+CD-PNIPAM₇₃**, **complex 2** was the proton signals of aromatic rings in the ternary system of **AZO+ Te-CD-PNIPAM₇₃**, and **complex 3** was the aromatic rings in the ternary system of **AZO+Arg-CD-PNIPAM₇₃** in D₂O. Comparing **complex 1** with **complex 2** or **complex 3**, we noticed that proton signals of c₁, a₁, b₁, h₁ in **complex 1** shifted to a low field, which suggested that these protons were exposed to water moderately. This phenomenon might be derived from the better solubility of **AZO** when it was included in the hydrophobic cavity of cyclodextrin. We also found that proton signals of d₁ and g₁ in **complex 1** shifted to a high field (proton signals of e₁ and f₁ were buried by the protons

of polymer), which suggested that these protons were included in the hydrophobic cavity of cyclodextrin and the proton signals were shielded. These results were in line with the previous investigation of the formation mechanism of host-guest complex between **AZO** and functional cyclodextrin^{45,61}. Additionally, compared with the proton signals of d₂ and g₂ (or d₃ and g₃) in **complex 2** or **complex 3**, these proton signals in **complex 1** were broad peaks, which also proved that these protons were included in the hydrophobic cavity of cyclodextrin. Similar result was also reported previously⁶². The investigation mentioned above suggested that **AZO** was included in the cavity of cyclodextrin in **complex 1** and was not included in the cavity of cyclodextrin in **complex 2** or **complex 3**. It also proved that the cavity of cyclodextrin in **Te-CD-PNIPAM₇₃** or **Arg-CD-PNIPAM₇₃** was occupied by adamantane in **ADA-Te** or **ADA-Arg**. Equally, it indirectly confirmed that host-guest complex in SGPx was formed.

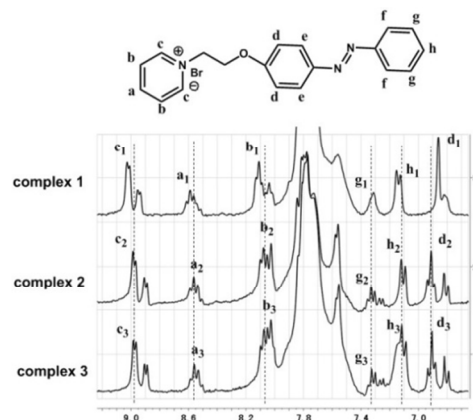


Fig. 3 ¹H NMR spectra of **complex 1**) the proton signals of aromatic rings in the binary system of **AZO+CD-PNIPAM₇₃**, **complex 2**) proton signals of aromatic rings in the ternary system of **AZO+ Te-CD-PNIPAM₇₃**, **complex 3**) aromatic rings in the ternary system of **AZO+ Arg-CD-PNIPAM₇₃** in D₂O.

Moreover, the formation of host-guest complex in **SGPx** was further confirmed by the changes of optical transmittance of various supramolecular building blocks (**CD-PNIPAM₇₃**, **Arg-CD-PNIPAM₇₃**, **Te-CD-PNIPAM₇₃**). As Fig. 4 displayed, the temperature dependence of optical transmittance of various supramolecular building blocks was given. Typically, The LCST of **CD-PNIPAM₇₃**, **Arg-CD-PNIPAM₇₃**, **Te-CD-PNIPAM₇₃** were 34.4°C, 33.6°C, 32.8°C, respectively. Compared with the LCST of **CD-PNIPAM₇₃**, the LCST of **Arg-CD-PNIPAM₇₃** (34.5°C) was higher and the LCST of **Te-CD-PNIPAM₇₃** (33.4°C) was lower. It was reported that the LCST of PNIPAM could be affected by the anchored functional groups with different hydrophilic-hydrophobic property⁶³. Herein, the phenomenon in this work was in good agreement with the previous report. It also proved that host-guest complex in **SGPx** was indeed formed.

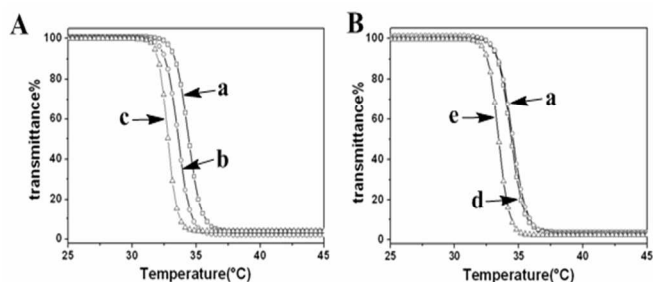


Fig. 4 Temperature dependence of optical transmittance at 600 nm obtained for pH 7.0, 50 mM PBS of (a) **CD-PNIPAM₇₃**, (b) **CD-PNIPAM₁₃₀**, (c) **CD-PNIPAM₃₇₄**, (d) **Arg-CD-PNIPAM₇₃**, (e) **Te-CD-PNIPAM₇₃** at concentration of 1 mg/ml

Optimizing the structure of smart artificial GPx

It is known that the slight change of the structure will result in dramatic change in catalytic activity for a native enzyme. Herein, both the polymer structure in **SGPx** and the match degree of the catalytic factors in **SGPx** played important roles in influencing the catalytic activity.

In the first place, as the cyclodextrin-containing host polymer (**CD-PNIPAM**) was used as scaffold for artificial GPx, it was necessary to reveal the influence of polymer structure on the catalytic activity of artificial GPx. Accordingly, three kinds of cyclodextrin-containing host polymers with different molecular weights (**CD-PNIPAM₇₃**, **CD-PNIPAM₁₃₀**, **CD-PNIPAM₃₇₄**) were synthesized by ATRP. Combining **CD-PNIPAMs** with **ADA-Te**, three kinds of host-guest artificial GPxs (**Te-CD-PNIPAM₇₃**, **Te-CD-PNIPAM₁₃₀**, **Te-CD-PNIPAM₃₇₄**) were constructed. Usually, the twine of polymer chain in PNIPAM was more serious when the molecular weight of PNIPAM was larger. Especially, during the temperature responsive process when the temperature was above LCST, the twine of polymer chain in PNIPAM was further enhanced. Therefore, we anticipated that the corresponding catalytic activities of **Te-CD-PNIPAM₇₃**, **Te-CD-PNIPAM₁₃₀**, **Te-CD-PNIPAM₃₇₄** could be affected by their different twisting polymer structures related to their different molecular weights.

To confirm this supposition and investigate the catalytic activities of **Te-CD-PNIPAM₇₃**, **Te-CD-PNIPAM₁₃₀**, **Te-CD-PNIPAM₃₇₄**, the temperature for the evaluating of catalytic

activity was firstly determined by the following way. As Fig. 4 a, b, c shown, the optical transmittance trend to be a fixed value when the temperature was above 36°C, which proved that the efficient self-assembled aggregation was formed during the temperature responsive process. Considering that self-assembly structure largely affected the catalytic activity of artificial GPx⁵⁰, the analysis of the catalytic activities was carried out at 36°C. For evaluating the catalytic behavior of **Te-CD-PNIPAM₇₃**, **Te-CD-PNIPAM₁₃₀**, **Te-CD-PNIPAM₃₇₄**, the catalytic activity for the reduction of cumene hydroperoxide (CUOOH) by 3-carboxyl-4-nitrobenzenethiol (TNB) was evaluated at 36°C according to the modified method reported by Hilvert et al¹² using TNB as a GSH alternative (see Fig. 5). The relative activities were summarized in Table 2. From Table 2, we found that the catalytic rates of **Te-CD-PNIPAM₇₃**, **Te-CD-PNIPAM₁₃₀**, **Te-CD-PNIPAM₃₇₄** were 2.02 $\mu\text{M}\cdot\text{min}^{-1}$, 1.51 $\mu\text{M}\cdot\text{min}^{-1}$, 1.41 $\mu\text{M}\cdot\text{min}^{-1}$, respectively. The catalytic rates decreased with the increasing molecular weights. This trend might be caused by their different temperature responsive properties related to their different molecular weights. Herein, the investigation of dynamic light scattering (Fig. 6 a, b, c) revealed that the hydrodynamic diameters was larger when the molecular weight was larger. Correspondingly, it meant that the aggregated morphology of **Te-CD-PNIPAM₃₇₄** was larger and the twine structure was much more serious. Under this condition, the catalytic center anchored in **Te-CD-PNIPAM₃₇₄** was easily buried in its twine structure when the temperature was above its LCST. This phenomenon might be responsible for the lower catalytic rate of **Te-CD-PNIPAM₃₇₄** and the higher catalytic rate of **Te-CD-PNIPAM₇₃**. Thus, **Te-CD-PNIPAM₇₃** was selected as the optimum host building block for the subsequently construction of **SGPx_{max}**.

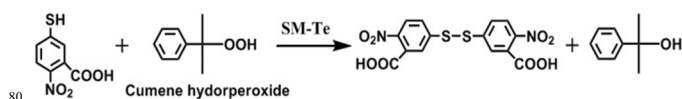


Fig. 5 Determination of GPx activity using 3-carboxyl-4-nitrobenzenethiol (TNB) as a substrate

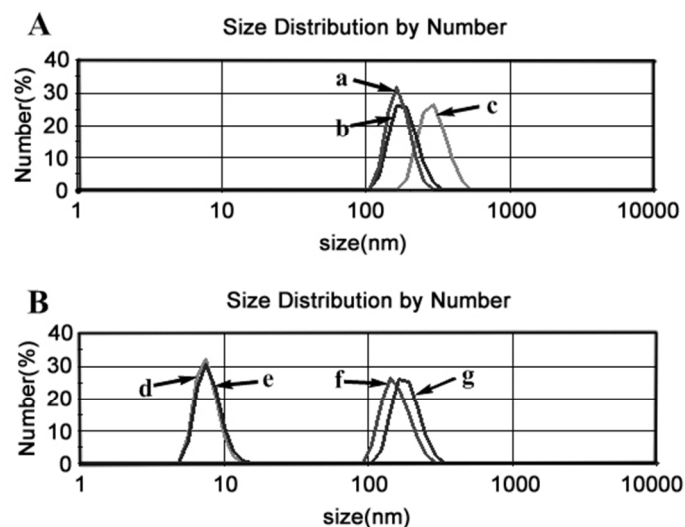


Fig. 6 A) Hydrodynamic diameters of **CD-PNIPAM₇₃**(a), **CD-PNIPAM₁₃₀**(b), and **CD-PNIPAM₃₇₄**(c) at 36°C determined using a Malvern ZETAS12-ERNANOSERIES instrument; B) Hydrodynamic diameters of **SGPx_{max}** at varying temperature (25°C(d); 32°C(e); 36°C(f); 40°C(g)).

Table 2 The initial rates (v_0) and activities for the reduction of hydroperoxides (ROOH) (250 μM) by ArSH in the presence of artificial GPx at pH 7.0 (50 mM PBS) and 36 $^\circ\text{C}$.

Catalyst	Temperature($^\circ\text{C}$)	ArSH	ROOH	$v_0(\text{mM}\cdot\text{min}^{-1})^a$
ADA-Arg	36	TNB	CUOOH	0.012
ADA-Te	36	TNB	CUOOH	0.23
CD-PNIPAM ₇₃	36	TNB	CUOOH	0.046
Arg-CD-PNIPAM ₇₃	36	TNB	CUOOH	0.018
Te-CD-PNIPAM ₇₃	36	TNB	CUOOH	2.02
Te-CD-PNIPAM ₁₃₀	36	TNB	CUOOH	1.51
Te-CD-PNIPAM ₃₇₄	36	TNB	CUOOH	1.41
Arg-Te-CD-PNIPAM _{73max}	36	TNB	CUOOH	9.36
CD-Te-CD-PNIPAM _{73max}	36	TNB	CUOOH	8.51
SGPx _{max}	36	TNB	CUOOH	18.75
SGPx _{max}	36	TNB	H ₂ O ₂	4.63
SGPx _{max}	36	NBT	CUOOH	8.12
SGPx _{max}	36	NBT	H ₂ O ₂	1.26

^aThe concentration of catalyst was 1 μM . And the initial rate of reaction was corrected for the spontaneous oxidation.

Subsequently, as the match degree of the catalytic factors in SGPx might play an important role in influencing the catalytic activity, the construction of optimum supramolecular artificial GPx (SGPx_{max}) was accomplished by a blending process. A graphical representation of the construction of SGPx_{max} was illustrated in Scheme 1 section 2. Herein, Te-CD-PNIPAM₇₃, Arg-CD-PNIPAM₇₃, and CD-PNIPAM₇₃ were functioned as the building blocks for SGPx_{max}, which endowed SGPx_{max} with the catalytic center, binding site, and hydrophobic cavity, respectively. Considering that the catalytic activity was crucial important for a successful artificial GPx, the data of the catalytic activities were employed as the effective values to reflect the optimization of artificial GPx by a blending process. On the one hand, by the blending of building blocks (Te-CD-PNIPAM₇₃ and Arg-CD-PNIPAM₇₃), Arg-Te-CD-PNIPAM₇₃ modified with catalytic center and binding site was constructed. As shown in Fig. 7 A, the component of Arg-Te-CD-PNIPAM₇₃ was

optimized by plotting the catalytic rate against the molar ratio of Arg-CD-PNIPAM₇₃ to Te-CD-PNIPAM₇₃. It was noticeable that the catalytic rate of Arg-CD-PNIPAM₇₃ increased to some extent with the molar ratio going up. And it reached the highest value (see Table 2, Arg-CD-PNIPAM_{73max}=9.36 $\mu\text{M}\cdot\text{min}^{-1}$) when the molar ratio was 6:1. However, the catalytic rate decreased when the molar ratio increased further. For Arg-CD-PNIPAM₇₃, the better match between catalytic center and binding site would result in the stronger substrate binding ability and higher catalytic activity. Thus, the highest catalytic activity was obtained when the best match was achieved with the molar ratio was 6:1. However, the enhanced binding ability could bind much more substrates in a distribution away from the catalytic center and made the completion of catalytic cycle in an inefficient way. Therefore, the decreased catalytic rate was observed when the molar ratio was increased further. Similar results were also reported in our previous work⁵⁰. On the other hand, using the same protocol as mentioned above, the component of CD-Te-CD-PNIPAM₇₃ was optimized by plotting the catalytic rate against the molar ratio of CD-PNIPAM₇₃ to Te-CD-PNIPAM₇₃ (see Fig. 7 B). And the highest catalytic rate (see Table 2, CD-Te-CD-PNIPAM_{73max}=8.51 $\mu\text{M}\cdot\text{min}^{-1}$) was achieved when the molar ratio of CD-PNIPAM₇₃ to Te-CD-PNIPAM₇₃ was 5:1.

Finally, the optimum SGPx was achieved using a blending process based on Te-CD-PNIPAM₇₃, Arg-CD-PNIPAM₇₃, and CD-PNIPAM₇₃. As displayed in Fig. 8, the molar ratio of Arg-CD-PNIPAM₇₃ to Te-CD-PNIPAM₇₃ was fixed to 6:1 and the molar ratio of CD-PNIPAM₇₃ to Te-CD-PNIPAM₇₃ was altered. Ultimately, the best match of catalytic factors was achieved by altering the molar ratio of three functional supramolecular polymers. The optimum SGPx (see Table 2, SGPx_{max}=18.75 $\mu\text{M}\cdot\text{min}^{-1}$) with the highest catalytic rate was successfully constructed when the molar ratio was 6:6:1. Now, we can draw a conclusion that the construction of SGPx_{max} was achievable through altering the molar ratio of three functional supramolecular polymers by a blending process.

Considering that detailed information of aggregated behavior of SGPx_{max} was important to reveal its catalytic mechanism, its detailed aggregated behavior was investigated based on dynamic light scattering, SEM, TEM and the temperature dependence of optical transmittance. As shown in Fig. 6 B, the hydrodynamic diameters of SGPx_{max} in aqueous solutions were typically 7 nm when the temperature was lower than the LCST of SGPx_{max} (curve d, curve e). Nevertheless, the corresponding hydrodynamic diameters shifted to larger than 100 nm when the temperature was higher than the LCST of SGPx_{max} (curve f, curve g). Considering that the hydrophilic PNIPAM block was changed to hydrophobic in different degree at corresponding temperature, the changes of the diameters of SGPx_{max} might be derived from the different assembled structures that were formed at corresponding temperatures. Similar phenomenon was also reported in our previous reports^{16,50}. Furthermore, the actual morphology of SGPx_{max} at 36 $^\circ\text{C}$ was observed by SEM in Fig. 9. We could clearly see that the presence of spherical nanoparticles of 80-100 nm in diameters. As SEM shown, the dimensions of these nanoparticles in the dry state were reasonably smaller than those detected by a Zetasizer Nano instrument at the same temperature, since the Zetasizer Nano

instrument provided the average hydrophobic diameter of nanoparticles in solution which contained the contribution from the swollen corona. Moreover, from the TEM image in Fig. 10, we found that the nanoparticles were hollow vesicle-like nanoparticles with a thinner region surrounded by a thicker region and clearly confirmed the boundary between the thinner and the thicker ones. Similar behavior has been reported by Chen and coworkers⁶⁴. Additionally, as Fig. 11 shown, the temperature dependence of optical transmittance of SGPx_{max} was given. Its LCST was 34.4°C

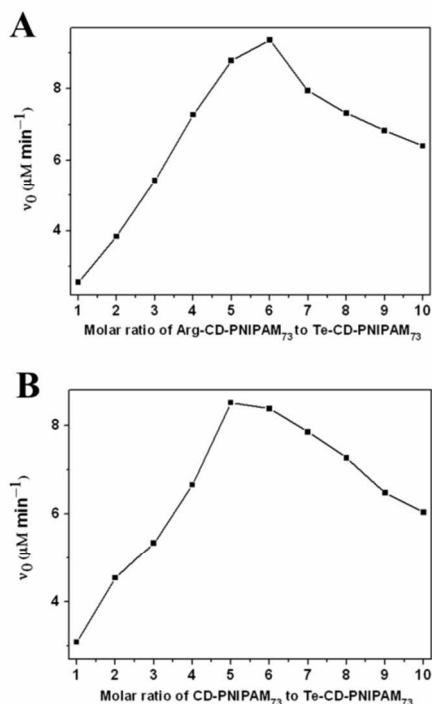


Fig. 7 Plots of catalytic rates v_0 against molar ratio of functional copolymer: (A) Arg-CD-PNIPAM₇₃ to Te-CD-PNIPAM₇₃ (The concentration of Te-CD-PNIPAM₇₃ was 1 μM . The concentrations of Arg-CD-PNIPAM₇₃ were 1, 2, 3, 4, 5, 6, 7, 8, 9, and 10 μM , respectively); (B) CD-PNIPAM₇₃ to Te-CD-PNIPAM₇₃ (The concentration of Te-CD-PNIPAM₇₃ was 1 μM . The concentrations of CD-PNIPAM₇₃ were 1, 2, 3, 4, 5, 6, 7, 8, 9, and 10 μM , respectively)

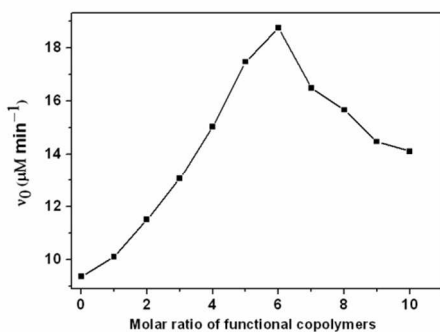


Fig. 8 Plots of catalytic rates v_0 against molar ratio of functional copolymer: (a) CD-PNIPAM₇₃ to Te-CD-PNIPAM₇₃ (the ratio of Arg-CD-PNIPAM₇₃ to Te-CD-PNIPAM₇₃ was fixed to 6:1). (The concentration of Te-CD-PNIPAM₇₃ was 1 μM . The concentrations of Arg-CD-PNIPAM₇₃ was 6 μM . The concentrations of CD-PNIPAM₇₃ were 0, 1, 2, 3, 4, 5, 6, 7, 8, 9, and 10 μM , respectively)

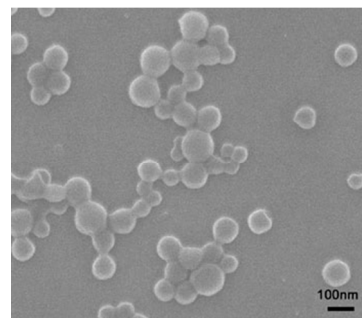


Fig. 9 SEM image for SGPx_{max} .

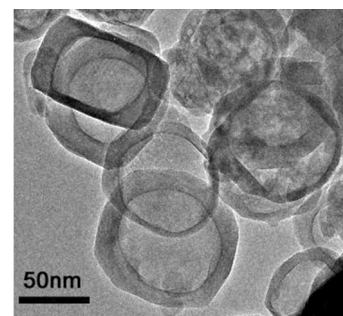


Fig. 10 TEM image for SGPx_{max} .

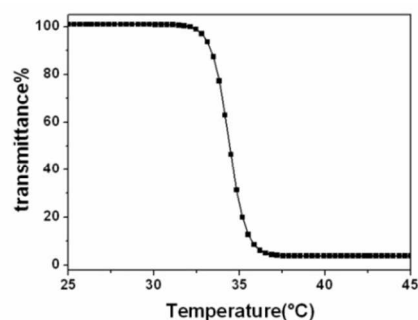


Fig. 11 Temperature dependence of optical transmittance at 600 nm obtained for pH 7.0, 50 mM PBS of SGPx_{max} at concentration of 1 mg/ml.

Catalytic behavior of SGPx_{max}

The catalytic activity of SGPx_{max} was investigated using TNB as a GSH alternative. Normally, the reaction between CUOOH and TNB was very slow under the spontaneous oxidation condition. To evaluate the influence of the catalytic activity by supramolecular scaffold, the control experiments were carried out. Typically, the catalytic activity of ADA-Arg, ADA-Te, CD-PNIPAM₇₃ and Arg-CD-PNIPAM₇₃ were determined using the similar assay method of other artificial enzyme (see Table 2). From Table 2, it was concluded that the reaction between CUOOH and TNB under the catalytic oxidation condition were relative lower. However, a remarkable rate enhancement ($\text{SGPx}_{\text{max}}=18.75 \mu\text{M}\cdot\text{min}^{-1}$) was observed under the identical condition when SGPx_{max} was added. This observation not only proved that the catalytic activities derived from the supramolecular scaffold were slight but also suggested that the remarkable catalytic activity can be obtained by assembly and blend of various catalytic element (catalytic center and binding site). Additionally, seen from Fig. 12, the saturation kinetic of SGPx_{max} for the peroxidase reaction was studied at the individual

concentrations of CUOOH, which indicated that **SGPx_{max}** exhibited typical saturation kinetics and acted as a real catalyst for peroxidase reaction. In the TNB assay system, the apparent kinetic parameters were obtained: $V_{\text{max}}=85.62 \mu\text{M}\cdot\text{min}^{-1}$, $k_{\text{cat}}^{\text{app}}=85.62 \text{ min}^{-1}$, $K_{\text{mCUOOH}}=907.53 \mu\text{M}$, $k_{\text{cat}}^{\text{app}}/K_{\text{mCUOOH}}=9.43\times 10^4 \text{ M}^{-1}\cdot\text{min}^{-1}$, and the turnover number per catalytic center tellurium was calculated to be 86 min^{-1} .

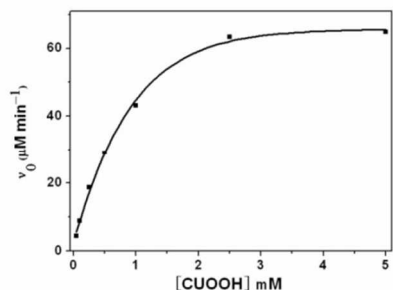


Fig. 12 Plots of initial rates at different concentrations of CUOOH in the presence of **SGPx_{max}**. The initial concentration of TNB was fixed to 0.15 mM, The concentrations of CUOOH were 0.05, 0.10, 0.25, 0.5, 1, 2.5 and 5 mM, respectively

For an efficient artificial enzyme, the strong substrates binding ability was one of the most important characteristics. For native GPx, the binding site (formed between two arginines and carboxylic group of GSH) and the hydrophobic cavity (composed of some hydrophobic amino residues) played important roles in binding substrates and maintaining the efficient catalytic activity. For **SGPx_{max}** constructed in this work, similar binding site and hydrophobic cavity were also incorporated. Herein, the binding site was derived from the arginine residue in **ADA-Arg**. And the cavity of cyclodextrin in **CD-PNIPAM₇₃** could effectively recognize aromatic thiol substrates being similar to the hydrophobic cavity in native GPx. Consequently, the best match degree of catalytic factors (catalytic center, binding site, and hydrophobic cavity) might endow **SGPx_{max}** with strong and special substrates binding ability. Equally, it would also play an important role in maintaining the efficient catalytic activity.

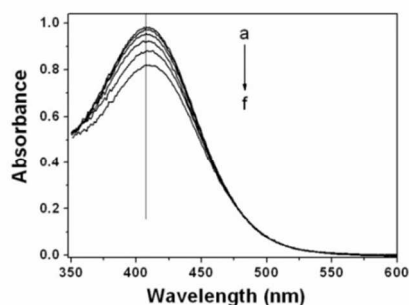


Fig. 13 UV spectra with varying concentration of **SGPx_{max}** in water; the concentration of TNB was 68 μM , and from a to f the concentrations of **SGPx_{max}** were 0, 0.2, 0.4, 1, 1.5, and 4 mM, respectively.

To confirm the interaction between the substrate TNB and **SGPx_{max}**, UV spectrum were employed to check the substrate binding ability. It was known that the maximum absorbance wavelength of TNB was 410 nm in aqueous solution (pH=7.0),

and it would appear as a red shift when it was in a hydrophobic microenvironment. Fig. 13 illustrated the UV spectra of the assayed mixtures with various amounts of **SGPx_{max}**. As expected, a red shift of maximum absorbance wavelength was observed, which indicated that a strong hydrophobic interaction existed between the aryl moiety of TNB and the binding sites of **SGPx_{max}**. In other words, **SGPx_{max}** could exhibit the strong substrates binding ability during the GPx catalytic process. To further confirm the substrate binding ability of **SGPx_{max}**, the catalytic rates were measured in different assay systems (shown in Fig. 14): CUOOH, TNB assay system (Fig. 14 A), $v_0=18.75 \mu\text{M}\cdot\text{min}^{-1}$; CUOOH, NBT assay system (Fig. 14 B), $v_0=8.12 \mu\text{M}\cdot\text{min}^{-1}$; H_2O_2 , TNB assay system (Fig. 14 C), $v_0=4.63 \mu\text{M}\cdot\text{min}^{-1}$; H_2O_2 , NBT assay system (Fig. 14 D), $v_0=1.26 \mu\text{M}\cdot\text{min}^{-1}$. It was found that much lower catalytic rate was observed when NBT was used as substrate (B<A or D<C). The difference between NBT and TNB was that NBT was a smaller molecule in size than TNB owing to the lack of a carboxyl function group in NBT. Considering that the similar assay condition (only substrates TNB and NBT were different) was used in two assay systems, the dramatic change in the catalytic activities should be mainly derived from the electrostatic interaction that was formed between the carboxyl in TNB and arginine in **SGPx_{max}**. Furthermore, the catalytic rates were measured under same condition except the different ROOHs (CUOOH and H_2O_2) were used. The difference between CUOOH and H_2O_2 was that CUOOH was a more hydrophobic substrate than H_2O_2 owing to the presence of the hydrophobic cumenyl group in CUOOH. Usually, the rate constants of the spontaneous reaction between hydroperoxide and thiol vary in magnitude in the order $k(\text{H}_2\text{O}_2) > k(\text{CUOOH})$ ⁷. However, by comparing the assay system A and C (or B and D), it was noticeable that the catalytic activity of **SGPx_{max}** exhibited a significant enhancement when CUOOH as a substrate instead of H_2O_2 . This difference in catalytic activities was mainly because that the hydrophobic microenvironment in **SGPx_{max}** enabled the hydrophobic substrate CUOOH to approach **SGPx_{max}** easier and complete the catalytic cycle more preferentially.

Consequently, based the above experiments, we could conclude that **SGPx_{max}** was endowed with strong substrate binding ability through both electrostatic interaction and hydrophobic interaction, which was derived from **Arg-CD-PNIPAM₇₃** and **CD-PNIPAM₇₃** respectively. And the stronger substrate binding ability further resulted in higher catalytic rates

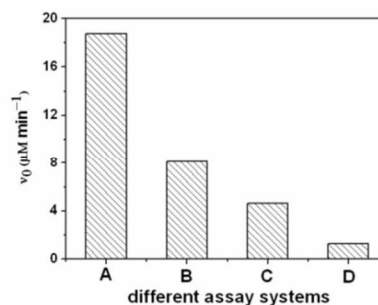


Fig. 14 The catalytic rates (v_0) for the reduction of hydroperoxides (250 μM) by TNB and NBT (150 μM) in the presence of **SGPx_{max}** at pH 7.0 (50 mM PBS) and 36°C. (A) CUOOH, TNB; (B) CUOOH, NBT; (C)

H₂O₂, TNB; (D) H₂O₂, NBT.

Temperature responsive catalytic behavior of SGPx_{max}

The temperature responsive property of SGPx_{max} was investigated by assaying the catalytic activities in TNB assay system using CUOOH as a substrate at various temperatures from 25°C to 45°C. To our knowledge, for the majority of temperature-activated reactions, the reaction rates would be enhanced with rising temperature according to Arrhenius equation. However, it was different for SGPx_{max}. Herein, a thermal-responsible catalytic activity curve was obtained by plotting the catalytic rate against temperature (Fig. 15).

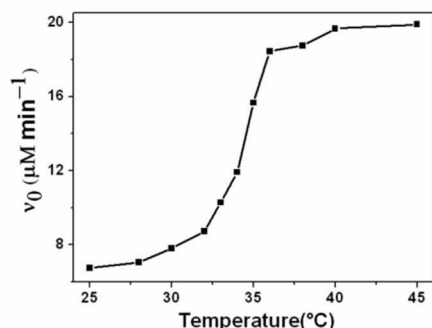


Fig. 15 Plots of the catalytic rate of SGPx_{max} (1.00 μM) versus temperature during the catalytic reduction of CUOOH (0.25 mM) by TNB (0.15 mM).

It was observed that the catalytic activity increased slowly with the increasing temperature when the temperature was lower than 33°C, and it increased remarkably with the temperature increasing from 33°C to 36°C. Furthermore, when the temperature increased higher above 36°C, the catalytic activity increased slowly again. Benefited from the presence of PNIPAM scaffold, SGPx_{max} exhibited the typical temperature responsive behavior. In the section *optimizing the structure of smart artificial GPx* mentioned above, the detailed information of aggregated behavior of SGPx_{max} during the temperature responsive process was investigated. We speculated that the temperature responsive catalytic activity of SGPx_{max} was endowed by the change of the self-assembled structure of SGPx_{max} during the temperature responsive process. To explicate the temperature responsive catalytic mechanism, the hydrodynamic diameters of the self-assembled structures of SGPx_{max} were assayed at various temperatures and the temperature dependence of optical transmittance of SGPx_{max} was measured with the increasing temperature. A graphical representation of the temperature responsive catalytic mechanism was illustrated in Scheme 1 section 3

Typically, PNIPAM exhibited the lower critical solution temperature (LCST) of about 32°C. A great deal of hydrogen bonds between amide group and surrounding water molecules were formed when the temperature was lower than its LCST, which enabled the PNIPAM block totally dissolve in water. However, the hydrophilic PNIPAM block changed to hydrophobic block to different degree when different amounts of hydrogen bonds were cleaved during the temperature responsive process. Usually, accompanied with break of hydrogen bonds, the self-

assembled structures were formed as the hydrophobic PNIPAM block aggregating together in water. And such phenomenon was also observed in the temperature responsive process of SGPx_{max} (its LCST was 34.4°C). As displayed in Fig. 11, the temperature dependence of optical transmittance of SGPx_{max} was measured at various temperatures from 25°C to 45°C. It was noticeable that the optical transmittance of SGPx_{max} was nearly 100% below 33°C, which indicated that SGPx_{max} was dissolved in water and the PNIPAM block was hydrophilic. Moreover, as shown in Fig. 6 B d and e, the hydrodynamic diameters of SGPx_{max} were smaller than 10 nm when the temperature was lower than its LCST, which also indicated that SGPx_{max} was hydrophilic and was dissolved in water. This observation was in close agreement with the analysis of the temperature dependences of optical transmittance of SGPx_{max}. Herein, for SGPx_{max}, the catalytic factors were incorporated into the supramolecular blocks. Therefore, the supramolecular blocks accompanied with catalytic factors were distributed in a randomly manner in water when the temperature was lower than its LCST. And the good match of the catalytic factors could not be easily achieved, which further resulted in a lower catalytic activity.

Subsequently, the sharp decrease in optical transmittance was observed in Fig. 11 when the temperature was higher than 33°C. The optical transmittance of SGPx_{max} became much lower with the increasing temperature, which indicated that the PNIPAM block of SGPx_{max} became hydrophobic due to the cleavage of hydrogen bonds. Meanwhile, the self-assembled structures were formed as the shift of PNIPAM in SGPx_{max} form hydrophilic to hydrophobic. From Fig. 6 B f and g, the increased hydrodynamic diameters of SGPx_{max} (larger than 100 nm) were observed when the temperature was higher than its LCST, which was in agreement with the conclusion from the changes of optical transmittance. Combing the detailed information of aggregated behavior from Fig. 9 and Fig. 10, it was concluded that self-assembled vesicles were formed when the PNIPAM block of SGPx_{max} changed from hydrophilic to hydrophobic. It is well known that a minor change of the the structure of the enzyme will result in a dramatic change in activity for naturally occurring enzymes. Herein, the remarkable changes of aggregated behavior of SGPx_{max} also resulted in a dramatic change in catalytic activity. As shown in Fig. 15, the curve of thermal-responsible catalytic activity was obtained by plotting the catalytic rate against temperature. The catalytic rate increased remarkably with the temperature increasing from 33°C to 36°C. Under these conditions, the PNIPAM block of SGPx_{max} was hydrophobic and the self-assembled vesicles were formed. Consequently, the catalytic factors in SGPx_{max} were concentrated in the vesicle, which resulted in the distance among the catalytic factors in vesicle was much closer. Accordingly, the better match of the catalytic factors could be easily achieved. Then, it enabled the catalytic cycle completed in an efficient way. Thus, as the better match of the catalytic factors were achieved with the temperature increasing from 33°C to 36°C, the largely enhancement of the catalytic activity was observed.

However, the catalytic activities increased slowly again when the temperature increased higher above 36°C. It was apparent that the optical transmittance of SGPx_{max} was stable when the temperature was above 36°C (see Fig. 11), which meant the

stable vesicles have aggregated under these conditions. As the cyclodextrin was anchored into **CD-PNIPAMs** as the end group, the catalytic factors were presented as the hydrophilic block at the end of functional building blocks (**CD-PNIPAM₇₃**, **Te-CD-PNIPAM₇₃**, **Arg-CD-PNIPAM₇₃**). Therefore, as illustrated in Scheme 1 **section 3**, these catalytic factors might be assembled on the surface of the aggregated vesicles as their hydrophilicity. Once the vesicle was formed, the distance of the catalytic factors would be slightly changed and the match degree of the catalytic factor changed to the steady state even if the temperature was further increased. Therefore, the substrates binding ability was also slightly changed and the catalytic activity was increased more slowly. Additionally, as shown in Fig. 6 B, the hydrodynamic diameter of **SGPx_{max}** was further increased at the higher temperature (**g>f**). It might be caused by the reason that the larger aggregated structure could be assembled by universal vesicles at higher temperature as the hydrophobicity of the PNIPAM became stronger, which was also reported in previous reported¹⁴. Under this condition, some catalytic factors might be buried in the scaffold of the larger aggregated structure, which would play a role in the slowly increasing of catalytic activity to some extent.

Now we can draw a conclusion that the change of the self-assembled structure of **SGPx_{max}** during the temperature responsive process plays a significant role in the altering of the temperature responsive catalytic activity.

Conclusions

In this work, a novel smart artificial GPx (**SGPx**) was prepared via host-guest interaction and a blending process for the first time. Herein, the functional guest molecules (**ADA-Te** and **ADA-Arg**) and the cyclodextrin-containing host polymers (**CD-PNIPAMs**) were synthesized. And the optimum host building block (**CD-PNIPAM₇₃**) was selected. Significantly, the optimum supramolecular artificial GPx (**SGPx_{max}**) with vesicles structure was achieved through altering the molar ratio of building blocks (**CD-PNIPAM₇₃**, **ADA-Te**, **ADA-Arg**). The catalytic rates of **SGPx_{max}** displayed a noticeable temperature responsive characteristic and **SGPx_{max}** exhibited the typical saturation kinetics behavior as a real enzyme catalyst. It was proved that the change of the self-assembled structure of **SGPx_{max}** during the temperature responsive process played a significant role in altering the temperature responsive catalytic behavior. We anticipate that this study would not only overcome the insurmountable disadvantages existed in traditional supramolecular artificial GPx but also open up a new field in designing other smart antioxidative artificial enzyme. And we also hope this prepared process could highlight the preparation of other biologically related functional supramolecular materials.

Acknowledgments

This research was supported by financial support from the Natural Science Foundation of China (No: 51303088, 51203082, 21234004), the Natural Science Foundation of Guangxi Province (No. 2013GXNSFBA019043), the Natural Science Foundation of Education Bureau of Guangxi Province (No. 2013YB254).

Notes and references

- a: School of Chemistry and Chemical Engineering, Qinzhou University, No.89, Xihuan Nanlu, Qinzhou 535000, People's Republic of China. E-mail:yinyanzhen2013@163.com; Fax: +86-0777-2860226
- b: State Key Laboratory of Supramolecular Structure and Materials, Jilin University, Changchun 130012, People's Republic of China E-mail:junqiu@jlu.edu.cn Fax: +8643185193421; † Electronic Supplementary Information (ESI) available: [The synthesis of **ADA-Te**, **ADA-Arg**, **CD-Br** and **CD-PNIPAM**]. See DOI: 10.1039/b000000x/
1. H. Sies, "Oxidative Stress: Introductory Remarks", in *Oxidative Stress*; Sies, H., Ed.; Academic Press:London, 1985, p. 1.
2. H. Sies, *Angew. Chem., Int. Ed. Engl.*, 1986, **25**, 1058-1071.
3. H. Sies, *Experimental physiology*, 1997, **82**, 291-295.
4. O. Epp, R. Ladenstein and A. Wendel, *Eur. J. Biochem.*, 1983, **133**, 51-69.
5. L. Flohé, G. Loschen, W. A. Günzler and E. Eichele, *Hoppe-Seyler's Z Physiol. Chem.*, 1972, **353**, 987-999.
6. T. G. Back and Z. Moussa, *J. Am. Chem. Soc.*, 2003, **125**, 13455-13460.
7. Z. Y. Dong, J. Q. Liu, S. Z. Mao, X. Huang, B. Yang, X. J. Ren, G. M. Luo and J. C. Shen, *J. Am. Chem. Soc.*, 2004, **126**, 16395-16404.
8. L. Engman, D. Stern, I. A. Cotgreave and C. M. Andersson, *J. Am. Chem. Soc.*, 1992, **114**, 9737-9743.
9. C. X. Hou, J. X. Li, L. L. Zhao, W. Zhang, Q. Luo, Z. Y. Dong, J. Y. Xu and J. Q. Liu, *Angew. Chem. Int. Ed.*, 2013, **52**, 5590-5593.
10. C. X. Hou, Q. Luo, J. Q. Liu, L. Miao, C. Q. Zhang, Y. Z. Gao, X. Y. Zhang, J. Y. Xu, Z. Y. Dong and J. Q. Liu, *ACS Nano*, 2012, **6**, 8692-8701.
11. G. Mugesh and H. B. Singh, *Chem. Soc. Rev.*, 2000, **29**, 347-357.
12. Z. P. Wu and D. Hilvert, *J. Am. Chem. Soc.*, 1990, **112**, 5647-5648.
13. Z. Y. Dong, Y. G. Wang, Y. Z. Yin and J. Q. Liu, *Curr. Opin. Colloid. In.*, 2011, **16**, 451-458.
14. X. Huang, Y. Z. Yin, X. Jiang, Y. Tang, J. Y. Xu, J. Q. Liu and J. C. Shen, *Macromol. Biosci.*, 2009, **9**, 1202-1210.
15. X. Huang, Y. Z. Yin, Y. Liu, X. L. Bai, Z. M. Zhang, J. Y. Xu, J. C. Shen and J. Q. Liu, *Biosens. Bioelectron.*, 2009, **25**, 657-660.
16. X. Huang, Y. Z. Yin, Y. Tang, X. L. Bai, Z. M. Zhang, J. Y. Xu, J. Q. Liu and J. C. Shen, *Soft Matter*, 2009, **5**, 1905-1911.
17. S. J. Yu, X. Huang, L. Miao, J. Y. Zhu, Y. Z. Yin, Q. Luo, J. Y. Xu, J. C. Shen and J. Q. Liu, *Bioorg. Chem.*, 2010, **38**, 159-164.
18. S. J. Yu, W. Zhang, J. Y. Zhu, Y. Z. Yin, H. Y. Jin, L. P. Zhou, Q. Luo, J. Y. Xu and J. Q. Liu, *Macromol. Biosci.*, 2011, **11**, 821-827.
19. S. J. Yu, Y. Z. Yin, J. Y. Zhu, X. Huang, Q. Luo, J. Y. Xu, J. C. Shen and J. Q. Liu, *Soft Matter*, 2010, **6**, 5342-5350.
20. Y. Z. Yin, X. Huang, C. Y. Lv, L. Wang, S. J. Yu, Q. Luo, J. Y. Xu and J. Q. Liu, *Macromol. Biosci.*, 2010, **10**, 1505-1516.
21. Y. Tang, L. P. Zhou, J. X. Li, Q. Luo, X. Huang, P. Wu, Y. G. Wang, J. Y. Xu, J. C. Shen and J. Q. Liu, *Angew. Chem. Int. Ed.*, 2010, **49**, 3920-3924.
22. H. Y. Wang, L. Wang, X. G. Wang, J. Y. Xu, Q. Luo and J. Q. Liu, *New J. Chem.*, 2011, **35**, 2632-2638.
23. A. Klug, *Angew. Chem., Int. Ed. Engl.*, 1983, **22**, 565-582.
24. J. M. Lehn, *Science*, 2002, **295**, 2400-2403.
25. C. Casati, P. Franchi, R. Pievo, E. Mezzina and M. Lucarini, *J. Am. Chem. Soc.*, 2012, **134**, 19108-19117.
26. J. M. Lehn, *Chem. Soc. Rev.*, 2007, **36**, 151-160.
27. J. M. Lehn, *Chem-Eur. J.*, 1999, **5**, 2455-2463.
28. T. Ogoshi, Y. Takashima, H. Yamaguchi and A. Harada, *J. Am. Chem. Soc.*, 2007, **129**, 4878-4879.
29. H. Yang, H. Chen and Y. B. Tan, *RSC Adv.* 2013, **3**, 3031-3037.
30. R. Bappaditya, B. Partha and K. N. Arun, *RSC Adv.* 2014, **4**, 1708-1734.
31. D. L. Wang, X. Y. Huan, L. J. Zhu, J. Y. Liu, F. Qiu, D. Y. Yan and X. Y. Zhu, *RSC Adv.* 2012, **2**, 11953-11962.
32. C. C. Neikirk, J. W. Chung and R. D. Priestley, *RSC Adv.* 2013, **3**, 16686-16696.

33. Y. Bai, Q. Luo, W. Zhang, L. Miao, J. Xu, H. Li and J. Liu, *J. Am. Chem. Soc.*, 2013, **135**, 10966-10969.
34. T. Kubori, Y. Matsushima, D. Nakamura, J. Uralil, M. Lara-Tejero, A. Sukhan, J. E. Galán and S. I. Aizawa, *Science*, 1998, **280**, 602-605.
35. P. Díez, R. Villalonga, M. L. Villalonga and J. M. Pingarrón, *J. Colloid. Interface. Sci.*, 2012, **386**, 181-188.
36. S. M. Reddy, Q. T. Phan, H. E. Sharif, L. Govada, D. Stevenson and N. E. Chayen, *Biomacromolecules*, 2012, **13**, 3959-3965.
37. L. Tan, Y. Liu, W. Ha, L. S. Ding, S. L. Peng, S. Zhang and B. J. Li, *Soft Matter* 2012, **8**, 4746-4749.
38. J. Li, X. Li, X. Ni, X. Wang, H. Li and K. W. Leong, *Biomaterials*, 2006, **27**, 4132-4140.
39. J. Yu, H. Fan, J. Huang and J. Chen, *Soft Matter*, 2011, **7**, 7386.
40. M. J. Robb, L. A. Connal, B. F. Lee, N. A. Lynd and C. J. Hawker, *Polym. Chem.*, 2012, **3**, 1618-1628.
41. B. Karagoz, L. Esser, H. T. Duong, J. S. Basuki, C. Boyer and T. P. Davis, *Polym. Chem.*, 2014, **5**, 350-355.
42. A. Harada, R. Kobayashi, Y. Takashima, A. Hashidzume and H. Yamaguchi, *Nat. Chem.*, 2010, **3**, 34-37.
43. M. Nakahata, Y. Takashima, H. Yamaguchi and A. Harada, *Nat Commun*, 2011, **2**, 511.
44. J. Q. Liu, G. M. Luo, S. J. Gao, K. Zhang, X. F. Chen and J. C. Shen, *Chem. Commun.*, 1999, 199-200.
45. Y. Z. Yin, S. F. Jiao, C. Lang, J. Q. Liu, *Soft Matter*, 2014, DOI:10.1039/C3SM53117A
46. Z. Y. Dong, Q. Luo and J. Q. Liu, *Chem. Soc. Rev.*, 2012, **41**, 7890-7908.
47. Y. Z. Yin, Z. Y. Dong, Q. Luo and J. Q. Liu, *Prog. Polym. Sci.*, 2012, **37**, 1476-1509.
48. L. Yu, K. Dean and L. Li, *Prog. Polym. Sci.*, 2006, **31**, 576-602.
49. E. S. Gil, D. J. Frankowski, M. K. Bowman, A. O. Gozen, S. M. Hudson and R. J. Spontak, *Biomacromolecules*, 2006, **7**, 728-735.
50. Y. Z. Yin, L. Wang, H. Y. Jin, C. Y. Lv, S. J. Yu, X. Huang, Q. Luo, J. Y. Xu and J. Q. Liu, *Soft Matter*, 2011, **7**, 2521-2529.
51. C. Koopmans and H. Ritter, *Macromolecules*, 2008, **41**, 7418-7422.
52. M. Ciampolini and N. Nardi, *Inorg. Chem.*, 1966, **5**, 41-44.
53. G. Masci, L. Giacomelli and V. Crescenzi, *Macromol. Rapid Commun.*, 2004, **25**, 559-564.
54. T. M. Eggenhuisen, C. R. Becer, M. W. Fijten, R. Eckardt, R. Hoogenboom and U. S. Schubert, *Macromolecules*, 2008, **41**, 5132-5140.
55. J. Wang and K. Matyjaszewski, *J. Am. Chem. Soc.*, 1995, **117**, 5614-5615.
56. K. Matyjaszewski and J. Xia, *Chem. Rev.*, 2001, **101**, 2921-2990.
57. D. G. Lessard, M. Ousalem and X. X. Zhu, *Can. J. Chem.*, 2001, **79**, 1870-1874.
58. Y. Xia, X. Yin, N. A. D. Burke and H. D. H. Stöver, *Macromolecules*, 2005, **38**, 5937-5943.
59. C. Alexander and K. M. Shakesheff, *Adv. Mater.*, 2006, **18**, 3321-3328.
60. T. Rossow, S. Bayer, R. Albrecht, C. C. Tzschucke and S. Seiffert, *Macromol. Rapid Commun.*, 2013, **34**, 1401-1407.
61. P. Wu, R. Xiao, C. Zhang, L. Zhou, Q. Luo, J. Xu and J. Liu, *Catal. Lett.*, 2010, **138**, 62-67.
62. X. Liao, G. Chen, X. Liu, W. Chen, F. Chen and M. Jiang, *Angewandte Chemie*, 2010, **122**, 4511-4515.
63. H. Ringsdorf, J. Venzmer and F. Winnik, *Macromolecules*, 1991, **24**, 1678-1686.
64. M. Hua, T. Kaneko, X. Liu, M. Q. Chen and M. Akashi, *Polym. J.*, 2005, **37**, 59-64.

A smart supramolecular artificial glutathione peroxidase (**GPx**) with tunable catalytic activity was prepared based on host-guest interaction and a blending process. The change of the self-assembled structure of **SGP_x_{max}** during the temperature responsive process played a significant role in altering the temperature responsive catalytic behavior.

